PAPER • OPEN ACCESS

Understanding the heating mechanism of the solar active region atmosphere in chromosphere

To cite this article: Mehmet Sarp Yalim et al 2023 J. Phys.: Conf. Ser. 2544 012006

View the article online for updates and enhancements.

You may also like

- Three-dimensional Simulations of Magnetospheric Accretion in a T Tauri Star: Accretion and Wind Structures Just Around the Star Shinsuke Takasao, Kengo Tomida, Kazunari Iwasaki et al.
- Neutron guide shielding for the BIFROST spectrometer at ESS
 K. Mantulnikovs, M. Bertelsen, C.P. Cooper-Jensen et al.
- The effect of single and double vacancy on hydrogenated graphene for hydrogen storage application M S Yahya, G K Sunnardianto and M Handayani

2544 (2023) 012006 doi:10.1088/1742-6596/2544/1/012006

Understanding the heating mechanism of the solar active region atmosphere in chromosphere

Mehmet Sarp Yalim¹, Gary Zank^{1,2} Christian Beck³, Debi Prasad Choudhary⁴, Avijeet Prasad⁵, Qiang Hu^{1,2}, and Makayla Frisse¹

- ¹ Center for Space Plasma and Aeronomic Research, The University of Alabama in Huntsville, 320 Sparkman Drive, Huntsville, AL 35805, USA
- 2 Department of Space Science, The University of Alabama in Huntsville, 320 Sparkman Drive, Huntsville, AL 35805, USA
- ³ National Solar Observatory (NSO), 3665 Discovery Drive, Boulder, CO 80303, USA
- 4 Department of Physics and Astronomy, California State University, Northridge (CSUN), Northridge, CA 91330-8268, USA
- ⁵ Rosseland Centre for Solar Physics, University of Oslo, Postboks 1029, Blindern NO-0315, Oslo, Norway

E-mail: msy0002@uah.edu,garyp.zank@gmail.com,cbeck@nso.edu, debiprasad.choudhary@csun.edu,avijeet.prasad@astro.uio.no,qh0001@uah.edu, mpf0004@uah.edu

Abstract. Understanding the mechanisms underlying the heating of the solar atmosphere is a fundamental problem in solar physics. In this paper, we present an overview of our research on understanding the heating mechanism of the solar active region atmosphere in chromosphere. We investigate Joule heating due to the dissipation of currents perpendicular to the magnetic field by the Cowling resistivity using a data-constrained analysis based on observational and tabulated theoretical/semi-empirical solar atmosphere model data. As target region, we focus on a sunspot umbral light bridge where we find that this heating mechanism plays an important role and is also highly dynamic.

1. Introduction

One of the fundamental problems in solar physics is to determine the physical processes that maintain the thermal structure of the solar atmosphere [1]. There are various mechanisms attributed to the energy transfer throughout the solar atmosphere. In this paper, we investigate a mechanism that heats the solar active region atmosphere in chromosphere: Joule heating due to the dissipation of electric currents by magnetic resistivity, namely Cowling resistivity.

The energy transfer in the chromosphere can be attributed to a number of mechanisms such as Alfvén waves [2, 3], nanoflares [4, 5], Ellerman bombs (EBs) [6, 7], spicules [8, 9], and magneto-acoustic shocks [10]. [11, 12] suggested that the heating of the chromosphere is due to the dissipation of acoustic waves, which has, however, been questioned by [13, 14, 15].

Another candidate to heat the solar chromosphere would be resistive Ohmic dissipation [16, 17]. The plasma in the chromosphere is not fully ionized and ions and neutrals exist simultaneously. Cowling resistivity follows the interactions between ions and neutrals. It is a function of the plasma bulk density, temperature, magnetic field, as well as the ion and electron number densities. The Joule heating mechanism that we focus on results from the

Content from this work may be used under the terms of the Creative Commons Attribution 3.0 licence. Any further distribution of this work must maintain attribution to the author(s) and the title of the work, journal citation and DOI.

2544 (2023) 012006

doi:10.1088/1742-6596/2544/1/012006

dissipation of electric currents that are perpendicular to the magnetic field due to Cowling resistivity. This mechanism is represented by the generalized Ohm's law as a function of Cowling resistivity and electric current perpendicular to the magnetic field. We perform a dataconstrained analysis [18, 19] to calculate the Cowling resistivity and hence the Joule heating rate in a solar active region atmosphere based on tabulated data of stratified bulk plasma, ion and electron number densities, and temperature profiles from the tabulated data of five different theoretical/semi-empirical solar atmosphere models, namely the Maltby M model [20] for sunspot umbrae, the VAL C model [21] and the Harvard-Smithsonian Reference Atmosphere (HSRA) model [22] for quiet Sun, the VAL F model [21] for bright filament networks, and the Ding & Fang model [23] for sunspot penumbrae, in combination with the application of a nonforce-free-field (NFFF) magnetic field extrapolation technique [24, 25, 26] to the photospheric vector magnetic field data observed by the Helioseismic and Magnetic Imager (HMI) [27] magnetogram onboard Solar Dynamics Observatory (SDO) [28] to obtain the magnetic field. In addition, we also use temperature data from the inversion of spectroscopic data obtained by the Interferometric BI-dimensional Spectrometer (IBIS) instrument [29] at the ground-based Dunn Solar Telescope (DST) to further constrain our data analysis, and hence decrease the reliance of our analysis on the tabulated data from static solar atmosphere models.

The occurrence of dynamic phenomena in the chromosphere and transition region has been attributed to plasma heating by the formation of current sheets when a discontinuity in the 3D magnetic field arises [30, 31]. We focus on discontinuities in the magnetic field topology which produce electric currents that can heat the plasma in those regions by dissipation through the Cowling resistivity. Such currents can occur at all locations with strong gradients in the magnetic field strength or orientation. These conditions are prevalent for instance near light bridges (LBs) inside the umbra of sunspots, for magnetic flux emergence into a field-free or magnetic environment, near polarity inversion lines or near magnetic reconnection sites like EBs. In this paper, we analyze Joule heating in a sunspot umbral LB in NOAA AR 12002 on 2014 March 13 from 20:44 to 21:00 UT by applying the data-constrained analysis mentioned above.

Section 2 presents an overview of our data-constrained analysis to investigate the effects of Cowling resistivity on heating in the weakly-ionized chromosphere. Section 3 shows the results obtained for the Joule heating of a sunspot umbral LB. Finally, section 4 presents our conclusions.

2. Data-constrained analysis of Joule heating in the chromosphere

To describe the interaction of the chromospheric plasma with the magnetic field, and its dependence on the degree of collisional coupling, we apply a quasi-MHD single fluid theory complemented with a generalized Ohm's law as in [32]. Here, we will present a brief overview about how to calculate the Cowling resistivity. The details of the chromosphere model utilized can be found in [18].

Our main focus is on the calculation and effects of Cowling resistivity. The anisotropic dissipation of currents due to the presence of Cowling resistivity can be seen in the induction and energy equations given in Eq. 1 and Eq. 2, respectively, that illustrate the impact of the presence of neutrals through the terms that contain η_C :

$$\frac{\partial \mathbf{B}}{\partial t} + \nabla \cdot (\mathbf{v}\mathbf{B} - \mathbf{B}\mathbf{v}) + \nabla \times \eta J_{\parallel} + \nabla \times \eta_C J_{\perp} = 0, \tag{1}$$

and

$$\frac{\partial E}{\partial t} + \nabla \cdot \left[(E + p + \frac{B^2}{8\pi}) \mathbf{v} - \frac{\mathbf{B}}{4\pi} (\mathbf{v} \cdot \mathbf{B}) \right] - \nabla \cdot (\mathbf{B} \times \eta J_{\parallel}) - \nabla \cdot (\mathbf{B} \times \eta_C J_{\perp}) = \rho(\mathbf{v} \cdot \mathbf{g}) + S_{NA}. \tag{2}$$

Here, η is the Coulomb resistivity, η_C is the Cowling resistivity, J_{\parallel} and J_{\perp} are the components of current density parallel and perpendicular to the magnetic field **B**, E, p, ρ , **v**, and **g** are specific

2544 (2023) 012006

doi:10.1088/1742-6596/2544/1/012006

total energy, thermal pressure, density, velocity, and gravitational acceleration, respectively, and S_{NA} is the combination of non-adiabatic source terms corresponding to viscous heating, shock heating, thermal conduction, radiative transfer, and coronal heating.

To calculate the Cowling resistivity, η_C , we solve the following relation between the Cowling and Coulomb resistivities:

$$\frac{\xi_n^2 B_0^2}{\alpha_n} = \eta_C - \eta,\tag{3}$$

where B_0 is the magnetic field strength, ξ_n is an estimate for the neutral fraction which is a function of density and temperature, and α_n is also a function of density and temperature.

To calculate the Coulomb and Cowling resistivities, we need the magnetic field \mathbf{B} , the plasma bulk density ρ and temperature T as well as the ion and electron number densities, n_i and n_e , in the chromosphere. We calculate the 3D spatial variation of T in the vicinity of the target structure of interest (i.e., in this paper, a sunpot umbral LB) in the chromosphere by using the Calcium Inversion based on a Spectral ARchive (CAISAR) code [33, 34, 35] that inverts the spectroscopic data obtained from DST/IBIS. For the 1D variations of bulk plasma density ρ , electron number density n_e and the total hydrogen number density n_H with height above the photosphere, we use tabulated data from the Maltby-M, VAL C, VAL F, Ding & Fang, and HSRA atmosphere models. We then calculate n_i from n_e and n_H . Finally, the magnetic field \mathbf{B} is taken from the NFFF magnetic field extrapolation results.

It should be noted that we also have the option to use either the 1D stratified temperature profile with height from the tabulated model data or temperature data from inversion results of observations to test their effects on the analysis results.

After calculating the Cowling resistivity, we then calculate the electric currents from the gradients of the 3D extrapolated magnetic field topology to calculate the Joule heating from the generalized Ohm's law as $\eta_C J_{\perp}^2$.

3. Analysis of Joule heating in a sunspot umbral light bridge

As a primary target structure in our analysis, we focus on a sunspot umbral LB. LBs are elongated bright structures that are usually present during the early stages of sunspot formation or the late stages of sunspot decay and can have an umbral, penumbral or granular morphology [36]. They are relatively long-lived (hours to days) and less dynamic structures which makes them particularly suitable for heating by our proposed Joule heating mechanism. In [19], we demonstrated that the primary heating mechanism in a sunspot LB caused by flux emergence is Joule heating due to dissipation of currents by the Cowling resistivity based on our data-constrained analysis that involves data from observations and atmosphere models.

In this paper, we build on our analysis in [19], which utilized only magnetic field from observations while the rest of the plasma variables were taken from the tabulated data given by the Maltby M model including temperature, and present the effects of using the 3D spatial variation of temperature based on observational data on the Joule heating of the same LB.

We analyze observations of the leading sunspot in NOAA AR 12002 on 2014 March 13 from 20:44 to 21:00 UT, combining data from vector magnetograms observed by $SDO/{\rm HMI}$ SHARP data series and temperature data obtained by the inversion of spectroscopic data measured by $DST/{\rm IBIS}$ using the CAISAR inversion code. For more details about the data specifics, we refer the interested reader to [19].

Figure 1 (left panel) shows the field of view (FOV) of the HMI SHARP magnetogram (outer box) as well as the IBIS FOV (solid box) and a smaller FOV (dashed box) focusing on the LB. Our results are based on this smaller FOV.

In order to replace the tabulated temperature data with the observational temperature data in our analysis, it is necessary to assure the consistency between the observational temperature data and the rest of the plasma variables taken from tabulated solar atmosphere data. We have

2544 (2023) 012006

doi:10.1088/1742-6596/2544/1/012006

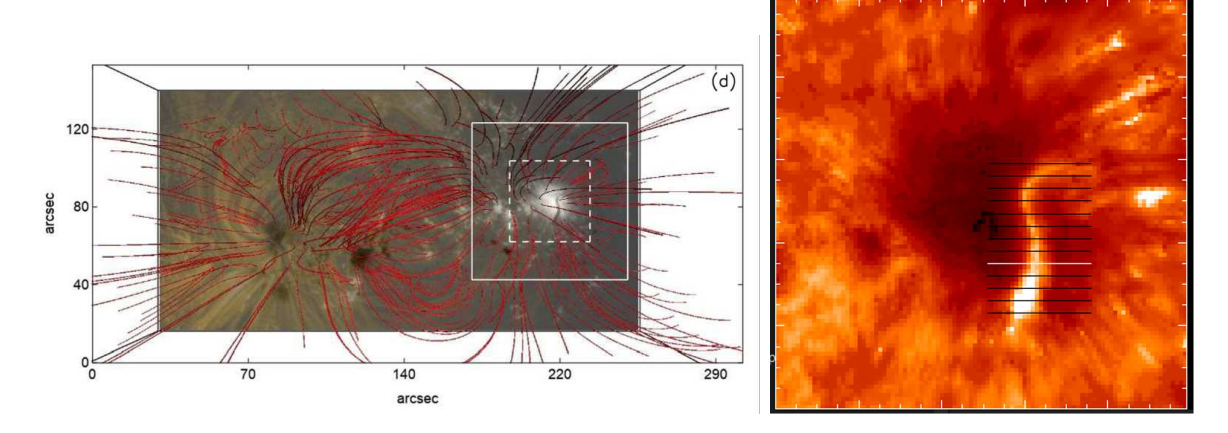


Figure 1. (Left panel) Field lines derived from the non-force-free field (NFFF) extrapolation overlaid on a composite image of the vertical component of the magnetic field and the AIA 171 Å image for the SHARP field of view (FOV) of AR 12002. The solid and dashed white squares correspond to the IBIS FOV and the smaller FOV shown in the right panel, respectively [19]; (Right panel) Spatial distribution of the LTE temperature from DST/IBIS data at z=0.36 Mm height above the photosphere in AR 12002. The white horizontal line marks slit No. 5 that crosses the LB.

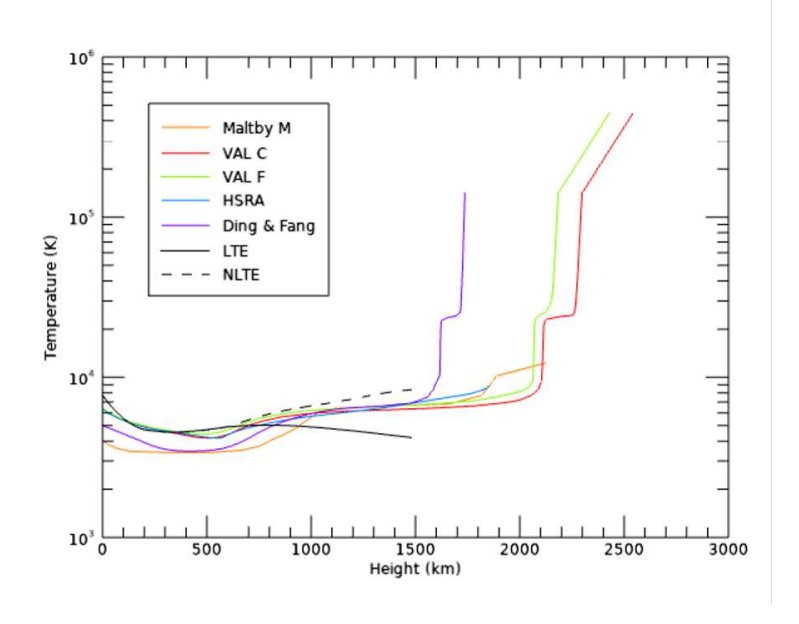


Figure 2. Temperature profiles in the chromosphere vs height above the photosphere from tabulated data of five solar atmosphere models. The LTE and NLTE temperature profiles are obtained from an inversion of spectroscopic data from DST/IBIS at the location where the height-averaged Joule heating rate distribution is maximum along the white slit shown in Figure 1 (right panel).

2544 (2023) 012006

doi:10.1088/1742-6596/2544/1/012006

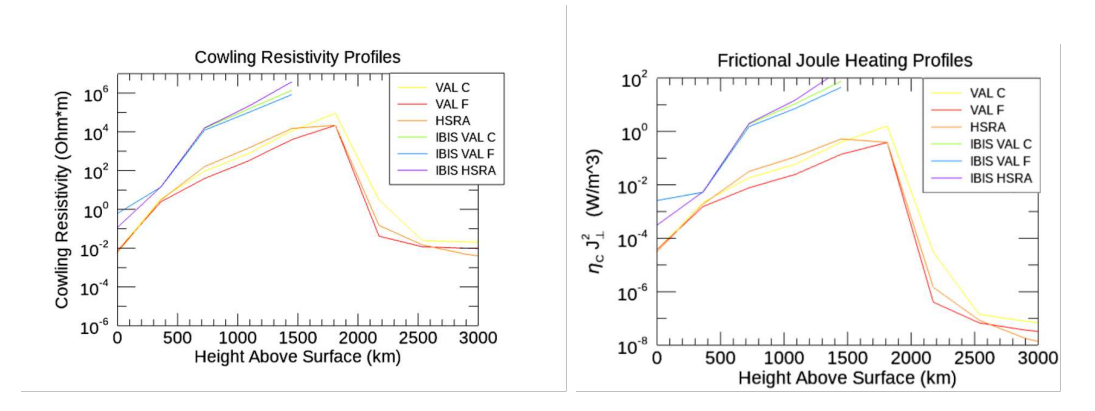


Figure 3. Variations of the maximum values of (Left panel) η_C and (Right panel) Joule heating rate profiles with height above the photosphere, calculated from VAL C, VAL F, and HSRA models with temperature from model or IBIS data. Both HMI and IBIS data correspond to AR 12002 at 21:00 UT.

five solar atmosphere models that model different types of regions of the solar active region atmosphere. In order to determine the model to use in our analysis, we compare the IBIS temperature data with the 1D stratified temperature variation with height from all five models as shown in Figure 2. We make this comparison at a representative location on the LB which is the location where the height-averaged Joule heating rate distribution is maximum along the white slit, which is shown in Figure 1 (right panel), that crosses approximately the center of the LB.

While we used Maltby-M model in our previous analysis in [19], the temperature data from IBIS that is obtained from the non-local thermodynamic equilibrium (NLTE) version of the inversion model, which is more accurate than the LTE version of the inversion model, agrees with the VAL F model the most, and also with the VAL C and HSRA models within 0-1,485 km height above the photosphere. We note that 1,485 km is the maximum height at which we obtain IBIS temperature data from the CAISAR inversion code.

Let us first have a look at the variations of Cowling resistivity and the associated Joule heating in the dashed box in Figure 1. Figure 3 shows the variations of the maximum values of η_C and the Joule heating rate with height above the photosphere using tabulated data or IBIS data for temperature in our analysis. For all three model selections to calculate the Cowling resistivity, namely VAL F, VAL C, and HSRA, using the 3D NLTE temperature distribution from IBIS instead of the 1D tabulated temperature profile leads to a Joule heating rate which is 2-3 orders of magnitude higher. This result already shows the impact of using observational temperature data in our analysis. We should, however, note that the locations of the maximum values of η_C and the Joule heating rate are not necessarily located on the LB at each height.

Let us now focus specifically on the LB. Figure 4 (left panel) shows the horizontal variations in the LTE and NLTE temperature data, averaged in height, across the center of the LB at the white slit. The middle and right panels in the same figure show the horizontal variations of the current perpendicular to the magnetic field J_{\perp} , η_C , and the Joule heating rate along the white slit. While η_C is calculated by plasma values from the VAL F model in both panels, tabulated temperature values are used in the middle panel whereas the inverted temperature values from IBIS are utilized in the right panel. While the distributions of all three quantities are qualitatively similar in both middle and right panels, quantitatively the maximum value of the Joule heating rate is 7 times higher when the IBIS temperature is used. In addition, the location of the peak of the NLTE temperature from IBIS coincides with the peak of the Joule

2544 (2023) 012006

doi:10.1088/1742-6596/2544/1/012006

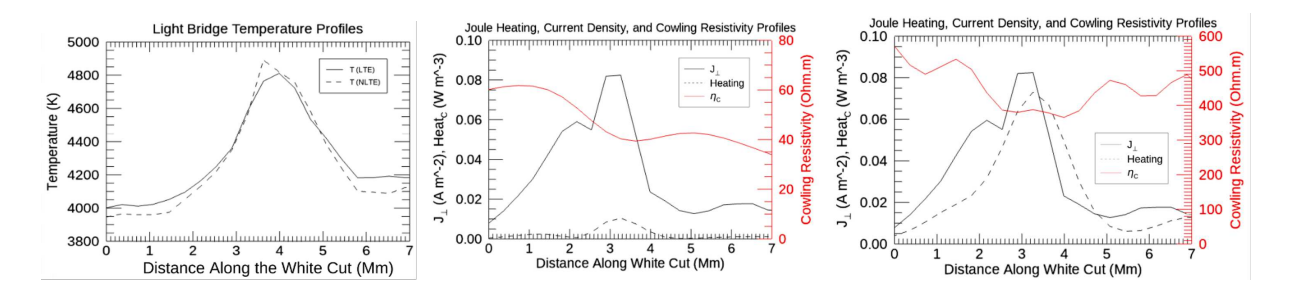


Figure 4. (Left panel) Horizontal variations in temperature from IBIS data, averaged in height, along the white slit shown in Figure 1 (right panel) across the LB; (Middle & right panels) Joule heating rate, J_{\perp} , and η_C profiles along the white slit. All three quantities are averaged in height up to 1,485 km. J_{\perp} has been scaled up by a factor of three and Joule heating rate has been scaled up by a factor of two. η_C is calculated based on the VAL F model using (Middle panel) tabulated temperature and (Right panel) observational temperature (NLTE) from IBIS. Both HMI and IBIS data correspond to AR 12002 at 20:48 UT.

heating rate which supports the role of our proposed Joule heating mechanism in the heating of the LB. If we look into the variations of the two terms that Joule heating is a function of, namely η_C and J_{\perp} , we see that η_C makes a dip and J_{\perp} has a peak at the peak location of the NLTE temperature from IBIS. This result indicates that the variation of J_{\perp} plays a major role in our proposed heating mechanism.

The results shown in Figure 4 are based on height averaging of the quantities across the white slit. How do η_C and the associated Joule (Ohmic) heating vary with height in the vicinity of the LB? Figure 5 presents the variations of these quantities at three different locations in the vicinity of the LB. The highly dynamic nature of the Joule heating can be clearly seen as the profiles in these locations look very different from each other both qualitatively and quantitatively.

Finally, let us make a quantitative comparison of the total Joule heating rate calculated by integrating the individual Joule heating rate values at each height at the location where the NLTE temperature from IBIS makes a peak along the white slit. Table 1 presents the Joule heating rate values obtained by using tabulated plasma variable values from each atmospheric model at two different times, namely 20:48 and 21:00 UT. Accordingly, the Joule heating rates are consistently larger at 21:00 UT than their values at 20:48 UT for each model which demonstrates that there is an ongoing heating event in the LB based on our proposed heating mechanism. The last two rows of the table show the results based on using tabulated and IBIS temperature data, respectively in our analysis. The total Joule heating rate at this location is 147 times larger at both times when we utilize the temperature variation from IBIS in our calculations. This result shows the importance of using observational data for temperature instead of tabulated data in our analysis and its impact on the results of our analysis.

4. Conclusions

In this paper, we investigate a mechanism that heats the solar active region atmosphere: Joule heating due to the dissipation of currents perpendicular to the magnetic field lines by Cowling resistivity in the chromosphere.

We give an overview of a data-constrained analysis to calculate the Cowling resistivity and the associated Joule heating. Our analysis can be constrained by both observational data (in particular, magnetic field from NFFF extrapolations applied to $SDO/{\rm HMI}$ magnetograms and temperature from the inversion of spectroscopic data from $DST/{\rm IBIS}$) and tabulated data from five distinct theoretical/semi-empirical solar atmosphere models corresponding to different

2544 (2023) 012006

doi:10.1088/1742-6596/2544/1/012006

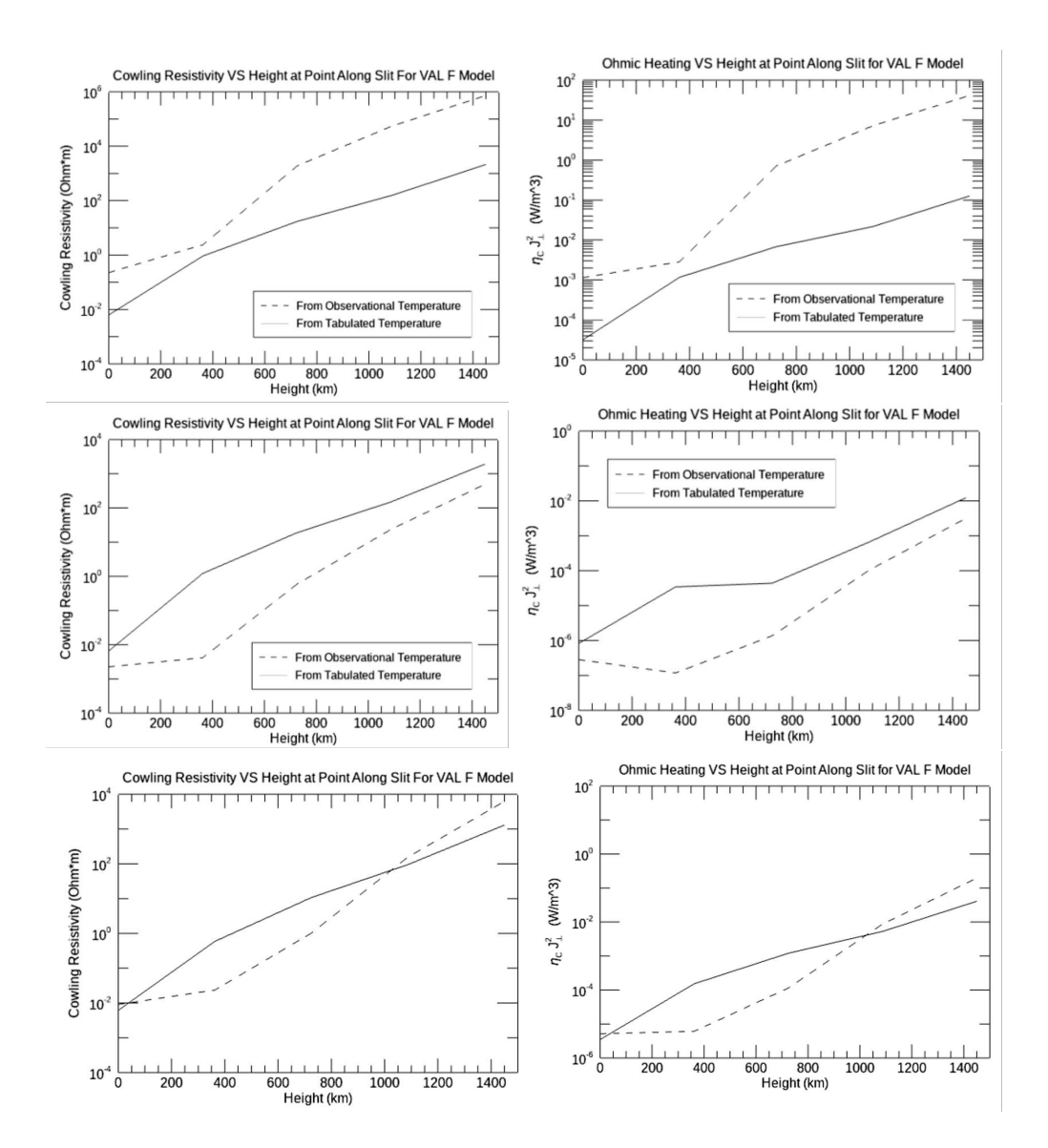


Figure 5. (Top panel) (Left) η_C and (Right) Joule heating rate variations with height at the location in the dashed line box in Figure 1 (left panel) where the NLTE temperature is maximum between the heights 1,000-1,500 km above the photosphere; (Middle panel) (Left) η_C and (Right) Joule heating rate variations with height at the center of the white slit in Figure 1 (right panel); (Bottom panel) (Left) η_C and (Right) Joule heating rate variations with height in the vicinity of the LB on the southernmost black slit in Figure 1 (right panel).

regions of the active region atmosphere. We analyze Joule heating over a sunspot umbral LB by using observational data for temperature and tabulated data for the rest of the plasma variables that are needed to calculate the Cowling resistivity from the VAL F model. VAL F is selected for our analysis since its 1D stratified temperature profile with height agrees the most with the NLTE temperature profile calculated from IBIS data at a representative point on the LB. We see a consistent increase of up to three orders of magnitude in the maximum values of Cowling resistivity and Joule heating rate at each height that are calculated using observational temperature instead of tabulated temperature from the VAL F, VAL C, and HSRA models. We observe an alignment of the height-averaged LTE and NLTE temperature, J_{\perp} , and the Joule

2544 (2023) 012006

doi:10.1088/1742-6596/2544/1/012006

Model	Height range (km)	$\begin{array}{c} \text{Joule heating rate} \\ \text{(W/m}^3\text{) (20:48 UT)} \end{array}$	$\begin{array}{c} \text{Joule heating rate} \\ \text{(W/m}^3\text{) (21:00 UT)} \end{array}$
Maltby M	0-2,500 km	1.2894	1.6812
VAL C	0-2,500 km	1.3542	1.8088
VAL F	0-2,500 km	0.3635	0.4847
HSRA	0-2,500 km	0.6846	0.9073
Ding & Fang	0-2,500 km	3.106	4.0749
VAL F	0-1,485 km	0.111	0.146
VAL F + IBIS	0-1,485 km	16.378	21.345

Table 1. The total Joule heating rate values between 0-2,500 km or 0-1,485 km height at the maximum height-averaged Joule heating location on the LB across the white cut in Figure 1 (right panel) for each model at 20:48 and 21:00 UT.

heating rate peaks across the LB. This demonstrates a strong dependence of heating on current, because the Joule heating rate makes a peak despite η_C having a local minimum at that location. We also observe higher values of up to 7 times for height-averaged Cowling resistivity and Joule heating rate when calculated with observational temperature data compared to those values when calculated with tabulated temperature from the VAL F model. We see that the total Joule heating rates at 21:00 UT are consistently greater than their values at 20:48 UT, and thus we can conclude that the LB experiences an ongoing heating event due to this mechanism. In particular, we observe that the total Joule heating rate values found using the NLTE temperature data from IBIS with the VAL F model are two orders of magnitude greater than their counterparts found using the VAL F model including the temperature. Finally, we find that the Joule heating rate is highly dynamic both on and in the vicinity of the LB from its variations with height at different locations. All the above observations support the importance of constraining our analysis using observational data. In particular, constraining temperature using observational temperature data from IBIS in our analysis is a major step forward from our last study [19]. In future work, we plan to calculate temperature and internal energy enhancements within the LB with respect to the umbral surroundings for quantitative validation for the same LB, and repeat our analysis on different target structures within the chromosphere.

Acknowledgments

We acknowledge support from the NSF EPSCoR RII-Track-1 Cooperative Agreements OIA-1655280 and OIA-2148653. We also acknowledge support from the NSF awards AGS-2020703 and AGS-2230633. M.F. acknowledges support from the NSF REU program under award number AGS-1950831. Any opinions, findings, and conclusions or recommendations expressed in this material are those of the author(s) and do not necessarily reflect the views of the National Science Foundation.

References

- [1] Narain U and Ulmschneider P 1996 Space Sci. Rev. 75 453
- [2] van Ballegooijen A A, Asgari-Targhi M, Cranmer S R and DeLuca E E 2011 Astrophys. J. 736 3
- [3] Sakaue T and Shibata K 2020 Astrophys. J. 900 120
- [4] Priest E R, Chitta L P and Syntelis P 2018 Astrophys. J. Lett. 862 L24
- [5] Syntelis P and Priest E R 2020 Astrophys. J. 891 52
- [6] Rutten R J 2016 A & A 590 A124

2544 (2023) 012006 doi:10.1088/1742-6596/2544/1/012006

- [7] Chen Y, Tian H, Peter H, Samanta T, Yurchyshyn V, Wang H, Cao W, Wang L and He J 2019 Astrophys. J. Lett. 875 L30
- [8] De Pontieu B, McIntosh S W, Hansteen V H and Schrijver C J 2009 Astrophys. J. 701 L1
- [9] Beck C, Rezaei R, Puschmann K G and Fabbian D 2016 Sol. Phys. 291 2281
- [10] De Pontieu B, McIntosh S, Martinez-Sykora J, Peter H and Pereira T M D 2015 Astrophys. J. Lett. 799 L12
- [11] Ulmschneider R, Schmitz F, Kalkofen W and Bohn H U 1978 A & A 70 487
- [12] Kalkofen W 2007 Astrophys. J. 671 2154
- [13] Athay R G and Holzer T E 1982 Astrophys. J. 255 743
- $[14]\;$ Beck C, Khomenko E, Rezaei R and Collados M 2009 A & A 507 453
- [15] Beck C, Rezaei R and Puschmann K G 2012 A & A 544 A46
- [16] Parker E N 1983 Astrophys. J. 264 635
- [17] Tritschler A, Uitenbroek H and Reardon K 2008 Astrophys. J. 686 L45
- [18] Yalim M S, Prasad A, Pogorelov N V, Zank G P and Hu Q Astrophys. J. Lett. 899 L4
- [19] Louis R E, Prasad A, Beck C, Choudhary D P and Yalim M S 2021 A & A 652 L4
- [20] Maltby P, Avrett E H, Carlsson M, Kjeldseth-Moe O, Kurucz R L and Loeser R 1986 Astrophys. J. 306 284
- [21] Vernazza J E, Avrett E H and Loeser R 1981 Astrophys. J. Suppl. Ser. 45 635
- [22] Gingerich O, Noyes R W, Kalkofen W and Cuny Y 1971 Sol. Phys. 18 347
- [23] Ding M D and Fang C 1989 A & A 225 204
- [24] Hu Q and Dasgupta B 2008 Sol. Phys. 247 87
- [25] Hu Q, Dasgupta B, Choudhary D P and Büchner J 2008 Astrophys. J. 679 848
- [26] Hu Q, Dasgupta B, DeRosa M L, Büchner J, and Gary G A 2010 J. Atmos. Sol. Terr. Phys. 72 219
- [27] Schou J et al 2012 Sol. Phys. 275 229
- [28] Pesnell W D, Thompson B J and Chamberlin P C 2012 Sol. Phys. 275 3
- [29] Cavallini F 2006 Sol. Phys. 236 415
- [30] Solanki S K, Lagg A, Woch J, Krupp N and Collados M 2003 Nature 425 692
- [31] Bahauddin S M, Bradshaw S J and Winebarger A R 2021 Nat. Astron. 5 237
- [32] Leake J E and Arber T D 2006 A & A 450 805
- [33] Beck C, Rezaei R and Puschmann K G 2013 A & A 549 A24
- [34] Beck C, Choudhary D P, Rezaei R and Louis R E 2015 Astrophys. J. 798 100
- [35] Beck C, Gosain S and Kiessner C 2019 Astrophys. J. 878 60
- [36] Louis R E, Beck C and Choudhary D P 2020 Astrophys. J. 905 153